

# Target/Background Classification Regularized Nonnegative Matrix Factorization for Fluorescence Unmixing

Binjie Qin, Member, IEEE, Chen Hu, and Shaosen Huang

**Abstract**—Nonnegative matrix factorization (NMF) is usually applied to multispectral fluorescence imaging for fluorescence unmixing. Unfortunately, most NMF-based fluorescence unmixing methods fail to take advantage of spatial information in data. Besides, NMF is an inherently ill-posed problem, which gets worse in the sparse acquisition of multispectral data (from a small number of spectral bands) due to its insufficient measurements and severe discontinuities in spectral emissions. To overcome these limitations by exploiting the spatial difference between multiple-target fluorophores and background autofluorescence (AF), we propose improved normalized cut to automatically classify all multispectral pixels into target fluorophores and background AF groups. We then initialize NMF by extracting the endmember spectra of target/background fluorescent components in the two groups, and impose a  $L_{1/2}$ -norm partial sparseness constraint on merely the abundances of target fluorophores within hierarchical alternating least squares framework of NMF. Experimental results based on synthetic and in vivo fluorescence data show the superiority of the proposed algorithm with respect to other state-of-the-art approaches.

**Index Terms**—Fluorescence spectra, insufficient measurements, multispectral imaging, nonnegative matrix factorization (NMF), partial sparseness constraint, signal decomposition, spatial information, target/background classification.

## I. INTRODUCTION

**I**N VIVO multispectral fluorescence imaging instrument has been widely used to measure and/or record cellular and subcellular biological processes in the life and medical sciences, such as drug discovery and disease diagnosis [1]. The vast majority of applications of in vivo fluorescence imaging are based on epi-illumination planar imaging, where the exciting source and detectors reside on the same side of the tissue and the measurements are acquired in reflectance mode. Given exciting light sources, different fluorophores

labeled with fluorescent dyes can emit fluorescence photons from visible to near-infrared wavelengths to generate multispectral images. The multispectral images involve multispectral pixels represented by vectors, with each component being a measurement corresponding to the specific wavelengths. This fluorescence imaging instrument enables the simultaneous use of multiple fluorophores to detect and localize particular components of complex biomolecular assemblies in their *in vivo* sample. For most fluorophores, emission spectra are distinct, but often overlap and become indistinguishable in the mixed multispectral images. Hence, spectral unmixing (SUM) [2] is necessary in the multispectral fluorescence imaging instrument to decompose the mixed multispectral images into a product of pure spectral signatures  $S$ , i.e., endmembers, and corresponding fractional abundance  $C$ , indicating the proportion of each endmember. If the endmember spectra are identified [3] in advance, can be easily estimated by the use of supervised SUM methods such as least squares method. However, the factory-provided reference endmember spectra used in the supervised SUM are uncertain and always require extensive calibration efforts for the endmember identification [3]. Therefore, the unsupervised SUM has been developed to simultaneously estimate the spectra and abundances without a priori knowledge about endmember spectra.

Manuscript received July 8, 2015; revised November 13, 2015; accepted November 16, 2015. Date of publication January 25, 2016; date of current version March 8, 2016. This work was supported in part by the National Natural Science Foundation of China under Grant 61271320 and Grant 60872102 and in part by the China Scholarship Council through the Small Animal Imaging Project under Grant 06-545. The Associate Editor coordinating the review process was Dr. Shervin Shirmohammadi.

The authors are with the School of Biological Engineering, Shanghai Jiao Tong University, Shanghai 200240, China (e-mail: bj Qin@sjtu.edu.cn).

Color versions of one or more of the figures in this paper are available online at <http://ieeexplore.ieee.org>.

Digital Object Identifier 10.1109/TIM.2016.2516318

In designing, implementing, and assessing the fluorescence imaging instrument, there are some practical challenges that must be overcome, among which the so-called autofluorescence (AF) [1], [4] can be produced by some proteins such as collagens and other biological materials when they are excited by appropriate visible light in vivo fluorescence imaging. Generally, AF originates from all possible background disturbances, which mainly include two kinds of sources [1], [4]: 1) the AF caused by the natural fluorescent molecules in tissue and food and 2) some instrument-based noise, shading, and leakage light from exciting filters. Therefore, AF stems from various sources covering large background areas, and has a dispersive spatial distribution. Furthermore, the AF wavelength ranging from 400 to 700 nm is overlapped with the emission spectra of most fluorophores. Due to these extensive overlaps occurring between the fluorophores and AF in the spatial and spectral distributions, it is difficult to blindly separate multiple fluorophores from AF when the AF is regarded as a constituent component by the current

unsupervised SUM methods. Alternatively, some hardware-based methods subtract an AF estimate from observation data after using extra excitation filters or extra unlabeled samples to acquire bare AF images [1], [4]. To successfully practice these methods, we must carefully match the specific sets with the spectral properties of both AF and fluorophores. In many cases, none of the mentioned methods in the institute can fully remove the AF from the fluorescence imaging.

As an unsupervised data decomposition (or blind source separation) technique, nonnegative matrix factorization (NMF) has been successfully applied to blindly separate several sources and signals in SUM [4], [5], biomedical source separation [6], [7], and nondestructive testing [8]. However, there are three shortcomings. First, NMF suffers from an ill convergence problem such that starting from different initial search points results in different values for the elements and matrices. Especially, the ill convergence problem becomes worse when there are insufficient measurements and low spectral resolutions in the sparse acquisition of multispectral fluorescence imaging data from a small number (e.g., 3D) of spectral bands. However, this sparse acquisition can be fast and cost-effective in clinical applications. Therefore, different NMF studies have proposed appropriate initial values [9] and some additional regularization constraints (such as sparseness [10], [11] and smoothness constraints [12]) to ensure the optimal NMF solution. Second, current NMF-based unmixed results. The most recent trend of utilizing sparseness constraints [10], [11] for strengthening part-based representation do not discriminate sparse components from nonsparse components, limiting unmixing accuracy when only some special targets of interest are sparse while

specific background component is nonsparse. In fluorescence imaging, some sparseness-constrained methods [4], [12], [13] update the whole abundance matrix of all components, that the abundance matrices of fluorescent targets and AF may interfere with each other in NMF. Third, NMF does not consider spatial information of neighboring pixels from specific components to find more intuitive and interpretable unmixing solution of abundance matrix.

To overcome these limitations of NMF, this paper proposes an unsupervised target/background classification regularized NMF (TBCR-NMF)<sup>1</sup> with partial sparseness constraint. The motivation is based on the following two facts. First, multiple fluorophores tend to locally accumulate in specific biological tissues so that their sparse spatial distributions are usually confined to relatively small areas, while background AF propagates at all directions and diffuses widely over large areas. This spatial distribution difference between multiple target fluorophores and background AF is preserved across the whole spectral bands, although the sparse acquisition introduces sharp discontinuity in the spectral emissions across the multiple spectral bands. Second, the set of pixels of the multiple localized fluorophores similarly exhibits high intensities within local patches and can be classified into a single target group, while the set of pixels in the large background areas contains low intensity pixels that can

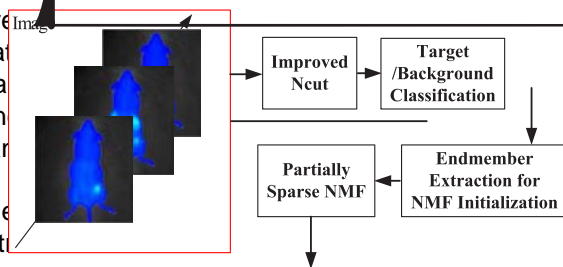
<sup>1</sup><http://www.escience.cn/people/bjqin/research.html>

As an excellent binary image segmentation algorithm, the original normalized cut (Ncut) [23] is done by partitioning all graph nodes (i.e., pixels) of whole image into

two disjoint parts. Rather than focusing on local features and their neighboring consistencies in the image data, Ncut aims at extracting the global impression of an image. It is assumed to be capable of utilizing the distinct global dissimilarities between target fluorophores and background AF in the whole fluorescence images to implement target/background segmentation. However, there are indeed more than two classes in the multispectral fluorescence images in the presence of multiple fluorophore targets. It is possible that the spectral emissions of some fluorescence targets are more similar to the AF spectral emission than other fluorescence targets. In this case, Ncut-based method will lead to a wrong target/background classification by grouping some fluorescence targets into the background AF group. To ensure accurate target/background classification, we modify classical Ncut method [23] to recursively repartition the large group of previous bipartition result if the number of groups segmented by Ncut is less than the number of endmembers in the fluorescence imaging. As a result, all the pixels of the multispectral images are classified into several groups, which further are simply merged into two main groups: the largest group is the background AF group and the rest of the smaller groups will join together into the target fluorescence group. Based on the improved Ncut-based classification, this paper has the following two contributions for the fluorescence SUM. First, by performing improved Ncut-based bipartitioning of target fluorescences and background AF groups, we propose target/background classification to benefit the endmember identification from the target and background groups for accurately initializing NMF. Second, this target/background classification facilitates imposing  $L_{1/2}$ -norm [24], [25] partial sparseness constraint on the abundances of the target fluorescent group but not on that of AF group in the NMF, which is based on hierarchical alternating least squares (HALS) framework. The remainder of this paper is organized as follows. Section II describes the idea and the details of the proposed SDR-NMF algorithm. Section III provides experimental results on synthetic and *in vivo* fluorescence imaging data. The conclusion and discussion are given in Section IV.

## II. MATERIALS AND METHODS

The fluorescence image data acquired with multispectral imaging instruments comprise four contiguous bands in this paper. A multispectral data set is usually stacked as an image cube and thus can be treated as a 3-D volumetric data set with two spatial axes (X and Y) and one spectral axis, as illustrated in Fig. 1. From a data-flow point of view, the flowchart of the proposed algorithm can be characterized as the following (see Fig. 1). First, a multispectral image cube is iteratively segmented into multiple separated homogeneous regions using the improved Ncut algorithm. Second, we further group these regions into target and background groups by classifying the largest region into the background group while merging all other small regions into the target group. Third, endmember extraction methods are employed to extract the spectral signatures of the target fluorescences and AF from the target and background regions for the NMF initialization.



where  $ass(A, V) = \sum_{u \in A, t \in V} w(u, t)$  is the total connections from nodes in  $A$  to all nodes in the graph and  $ass(B, V)$  is similarly defined. The Ncut grouping algorithm consists of the following steps. First, let  $H$  be an  $N \times N$  diagonal matrix with  $h$  on its diagonal and  $N$  be the number of the nodes and  $h(i) = \sum_j w(i, j)$ , where the weight  $w(i, j)$  is defined as  $w(i, j) = e^{-\frac{(\|x_i - x_j\|^2/\sigma)}$ , with  $x_i$  and  $x_j$  representing the normalized spectra of nodes  $i$  and  $j$ , which have zero-mean and unit variance, respectively. In addition,  $\eta = 0.1$  is a positive scaling factor determining the sensitivity of  $w(i, j)$  to the spectrum difference between nodes  $i$  and  $j$ ; Then, we solve  $(H - W)v = \eta Hv$  for eigenvectors  $v$  with the smallest eigenvalues  $\eta$ , where  $W$  is  $N \times N$  symmetric weight matrix with the element being  $w(i, j)$ . At last, use the second smallest eigenvector  $v_1$  and the splitting value 0.4 to bipartition graph, i.e., the bipartition is implemented by grouping the  $i$ th node into  $A$  if the  $i$ th component of eigenvector  $v_1$  is larger than 0.4,  $B$  otherwise.

For the multiple fluorophores in vivo fluorescence imaging, there are more than two classes in the fluorescence imaging. Therefore, the spectral emissions of some fluorescence targets are more similar to those of AF than other fluorescence targets, such that Ncut will lead to a wrong target/background classification by aggregating some fluorescence targets into the background AF group. To avoid this misclassification, we need to modify the recursive two-way Ncut method. Considering that background AF (including various background noises) has a dispersive spatial distribution while multiple fluorophores are locally accumulated at specific locations, we assume that the pure background AF regions are larger than the target fluorophore regions. Through Ncut-based bipartition, the larger group is either pure AF region or the regions that contain AF and some target fluorophores. In the latter case, the larger group will be bipartitioned again until all target fluorophores are separated from the AF region. Because the aim of the improved recursive Ncut method is to classify all pixels of the whole fluorescence region into two classes, background AF and target fluorescence groups, all the separated smaller regions except the largest AF region are finally combined together into the target fluorescence group.

Based on the above analysis, we propose an improved recursive Ncut method. First, to use the Ncut method, each  $992 \times 992$  spectral image is decimated into a size of  $100 \times 100$  pixels. Decreasing the number of graph nodes from near  $N = 1\,000\,000$  to  $N = 10\,000$  by this image subsampling can solve the large graph problem, which consumes too much memory and requires huge computational complexity in handling large-scale weight matrix  $W$  (with  $N \times N$  elements) for the graphical representation and generalized eigenvalue computation. In our experiments, changing image size from  $200 \times 200$  pixels to  $100 \times 100$  pixels can obviously decrease Ncut computation time from 56 to 28 s, but does not have an adverse effect on target/background classification, because the Ncut method's graph-based generalized eigenvalue computation is less sensitive to the spatial information lost during subsampling than other local feature-based segmentation. Besides, even if small noisy misclassification occurs, it cannot

affect the final TBCR-NMF's performance, because we only require an approximate global target/background classification for further decomposition refinement by TBCR-NMF itself. Second, after the initial Ncut-based bipartition, only the large cluster of the bipartition result will be chosen for subsequent bipartition. Third, we recursively repartition the large cluster of previous bipartition result if the number of intermediate clusters segmented by Ncut is less than the number of endmembers in the fluorescence imaging. Finally, the largest group is considered as the background AF group and all the rest of smaller groups are merged into the target fluorescence group. The intermediate target/background classification result after improved Ncut segmentation is shown in Fig. 1, where the different colors mean the different intermediate clusters sequentially segmented by the improved Ncut. The final target fluorescence group is formed by grouping all the small clusters except the large cluster of AF region.

B. Endmember Extraction for NMF Initialization

To find the optimal products that best approaches the mixed image data matrix  $D \in \mathbb{R}_+^{N \times L}$  ( $N$  is the total pixel number in a single image and  $L$  is the spectral band number), HALS-based NMF [26][28] is adopted to perform sequential constrained minimization on a set of subobjective functions  $F(C_{:,k}, S_{k,:}) = (1/2)\|R_k - C_{:,k} S_{k,:}\|_2^2$ , where each column  $C_{:,k}$  of  $C \in \mathbb{R}_+^{N \times K}$  represents the spatial distribution of one endmember component,  $K$  is the number of the endmember, and each row  $S_{k,:}$  of  $S \in \mathbb{R}_+^{K \times L}$  represents the spectrum of a specific endmember. For  $k = 1, 2, \dots, K$ ,  $R_k = D - \sum_{i \neq k} C_{:,i} S_{i,:}$ . To initialize NMF, we use the pixels of two groups to determine the corresponding spectra for the different fluorescence components. We assume that the first  $(K - 1)$  constituent components represent the fluorophores and the last component describes the AF. AF's initialized spectrum  $S_K$  is set to the average spectrum of all AF pixels, while the spectra  $S_1, S_2, \dots, S_{K-1}$

the  $L_{1/2}$ -norm as

$$F(\mathbf{C}_{:k}, \mathbf{S}_k) = \frac{1}{2} \|\mathbf{R}_k - \mathbf{C}_{:k} \mathbf{S}_k\|_2^2 + 2\theta \sum_{i=1}^N (\mathbf{C}_{ik})^{1/2} \quad (2)$$

where the  $\theta$  is a regularized parameter to balance the tradeoff between the approximation accuracy and the sparseness of the multiple fluorophores abundances. The gradient derivation of  $F(\mathbf{C}_{:k}, \mathbf{S}_k)$  with respect to  $\mathbf{C}_{:k}$  is

$$\frac{\partial F(\mathbf{C}_{:k}, \mathbf{S}_k)}{\partial \mathbf{C}_{:k}} = -(\mathbf{R}_k - \mathbf{C}_{:k} \mathbf{S}_k) \mathbf{S}_k^T + \theta (\mathbf{C}_{:k})^{-1/2} \quad (3)$$

where  $(\mathbf{C}_{:k})^{-1/2}$  is given by the element-wise square root for each entry in the vector  $\mathbf{C}_{:k}$ . By setting (3) to zero, we can get the updating rule of  $\mathbf{C}_{:k}$ . However, it involves a rather high computation cost due to the computation of the term  $(\mathbf{C}_{:k})^{-1/2}$ . To circumvent this problem, we approximate  $(\mathbf{C}_{:k})^{-1/2}$  term by its estimation  $\hat{\mathbf{C}}_{:k}$  obtained from the previous update, rather than compute the term  $(\mathbf{C}_{:k})^{-1/2}$  directly. Hence, (3) takes a simplified and more computationally efficient form

$$\frac{\partial F(\mathbf{C}_{:k}, \mathbf{S}_k)}{\partial \mathbf{C}_{:k}} = -(\mathbf{R}_k - \mathbf{C}_{:k} \mathbf{S}_k) \mathbf{S}_k^T + \theta \hat{\mathbf{C}}_{:k}^{-1/2}. \quad (4)$$

By setting (4) to zero, the rule of updating  $\mathbf{C}_{:k}$  takes the following form:

$$\mathbf{C}_{:k} = \max(\text{eps} (\mathbf{R}_k \mathbf{S}_k^T - \theta (\mathbf{C}_{:k})^{-1/2}) / \|\mathbf{S}_k\|_2^2) \quad (5)$$

where eps is a very small constant ( $10^{-16}$ ) and prevents from dividing by zero. The rules of updating  $\mathbf{S}_k$  for (2) is

$$\mathbf{S}_k = \max(\text{eps} \mathbf{C}_{:k}^T \mathbf{R}_k / \|\mathbf{C}_{:k}\|_2^2). \quad (6)$$

For  $k = K$ , the subobjective function has no sparseness constraint, and the corresponding updating rules are the same as the other parts of the HALS optimization.

For the convenience of parameter setting, we convert the regularized parameter  $\theta$  of TBCR-NMF into a desired sparsity value  $\phi$  [10], which represents the sparseness degree that we expect the abundances of multiple fluorophores to reach. The sparsity value  $\phi$ , being 0 for nonsparse results and 1 for extremely sparse results, can be defined as

$$\phi(\mathbf{C}_k) = \frac{\sqrt{N} - (\sum_{n=1}^N |c_{nk}| / \sqrt{\sum_{n=1}^N c_{nk}^2})}{\sqrt{N} - 1} \quad (7)$$

where  $\mathbf{C}_k \in \mathbb{R}_+^{N \times 1}$  is the  $k$ th column of abundance matrix  $\mathbf{C}$ , and  $c_{nk}$  is each element at  $\mathbf{C}_k$  with  $n = 1, 2, \dots, N$ . Specifically, for each fluorophore's abundance that has a corresponding regularized parameter  $\theta_k$ , we use a method similar to that in [31] to directly control the  $\theta_k$  value:  $\theta_k$  is initialized to 0.001, and after each iteration, the current sparsity  $\phi$  is computed by (7) for the abundance  $\mathbf{C}_k$ ; then  $\theta_k$  is increased by 5% if the current sparsity is less than the desired sparsity value  $\phi$ ; otherwise,  $\theta_k$  is decreased by 5%.

The detailed pseudocode of partially sparse NMF algorithm is summarized in Algorithm 1. The algorithm computation is terminated when the absolute value of difference between the two adjacent objective functions is less than  $10^{-4}$  or the maximum number of iterations exceeds 1000.

---

### Algorithm 1 Partially Sparse NMF

---

Input : Data matrix  $\mathbf{D} \in \mathbb{R}_+^{N \times L}$  and initial  $\mathbf{C} \in \mathbb{R}_+^{N \times K}$

---





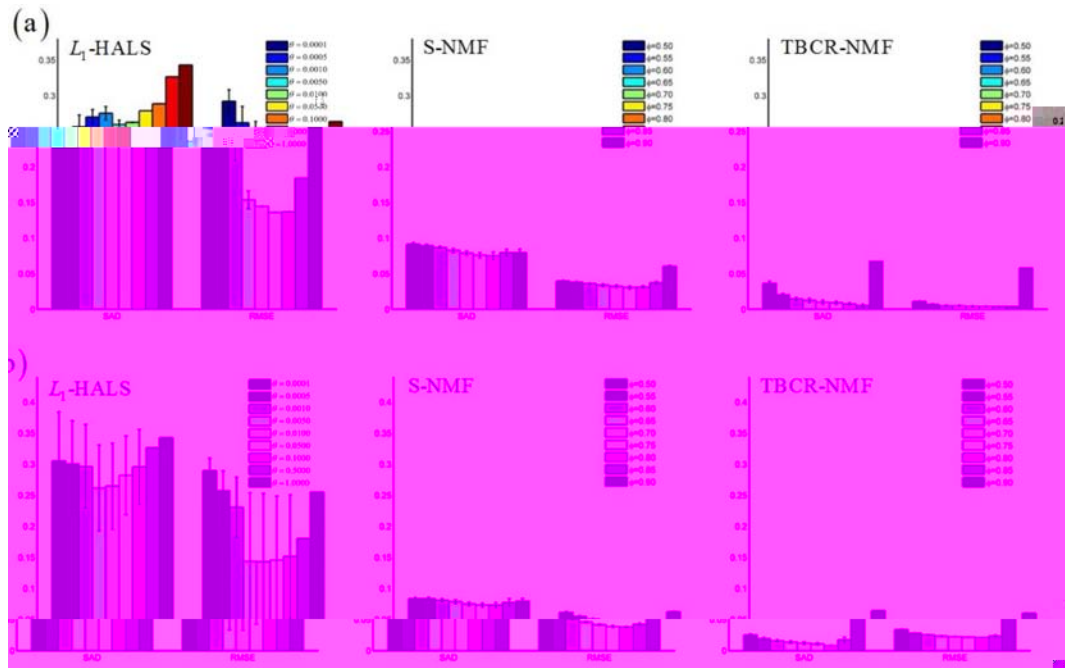


Fig. 3. Algorithm performances ( $\overline{SAD}$  and  $\overline{RMSE}$ ) for different values of parameter  $\theta$  and  $\phi$  when (a) no noise is added and (b) noise is added with SNR = 15 dB.

than 0.85, the  $\overline{SAD}$  and  $\overline{RMSE}$  become large and the unmixed results obtained with S-NMF, and Graph method for TBCR-NMF. Fig. 4(a) shows that the performances of  $\ell_1$ -HALS and S-NMF are worst compared with other results. However, TBCR-NMF is not sensitive to the AF/F ratio and obtains the smallest  $\overline{SAD}$  and  $\overline{RMSE}$  values in all different AF/F intensity ratios. However, TBCR-NMF obtains the smallest  $\overline{SAD}$  and  $\overline{RMSE}$  among the three algorithms when the sparsity  $\phi$  changes from 0.50 to 0.90 (or  $\theta$  changes from 0.0001 to 1.0000). When the sparsity  $\phi$  value is set to 0.90 (or  $\theta$  changes from 0.0001 to 1.0000), the poorest performances are achieved by all three algorithms, among which the TBCR-NMF is still the best.

The SNR in Fig. 3(b) is set to 15 dB, so that there is strong noise in the fluorescence data and the performance of all algorithms degrades with increasing noise levels. The proposed TBCR-NMF still achieves the smallest  $\overline{SAD}$  and  $\overline{RMSE}$  when  $\phi$  ranges from 0.5 to 0.9. The  $\overline{RMSE}$  achieved by TBCR-NMF is relatively steady when  $\phi$  ranges from 0.5 to 0.85. When the initial sparsity value exceeds the true sparsity (0.85), the values  $\overline{SAD}$  and  $\overline{RMSE}$  obtained by TBCR-NMF increase obviously, but are still smaller than those obtained by other algorithms. Therefore, TBCR-NMF can achieve the best unmixed results when there is strong noise in the fluorescence data.

As low AF/F ratio will highlight multiple localized fluorophores from the background AF, it essentially makes the mixed spectral data sparser than the high AF/F ratio and the corresponding NMF problem will have sparser solutions than the high AF/F ratio. Therefore, the NMF performance is largely dependent on the AF/F ratio. For simulation experiments, the AF/F intensity ratio ranges from 0.1 to 0.9 with interval of 0.2. The  $\phi$  and  $\theta$  parameters are set to 0.8 and 0.01, respectively, to achieve the best unmixing performance for all algorithms.

Fig. 4(a) shows the different  $\overline{SAD}$  and  $\overline{RMSE}$  values for the different AF/F intensity ratios in the noiseless data. The initialization is Random method for  $\ell_1$ -HALS, Pure method

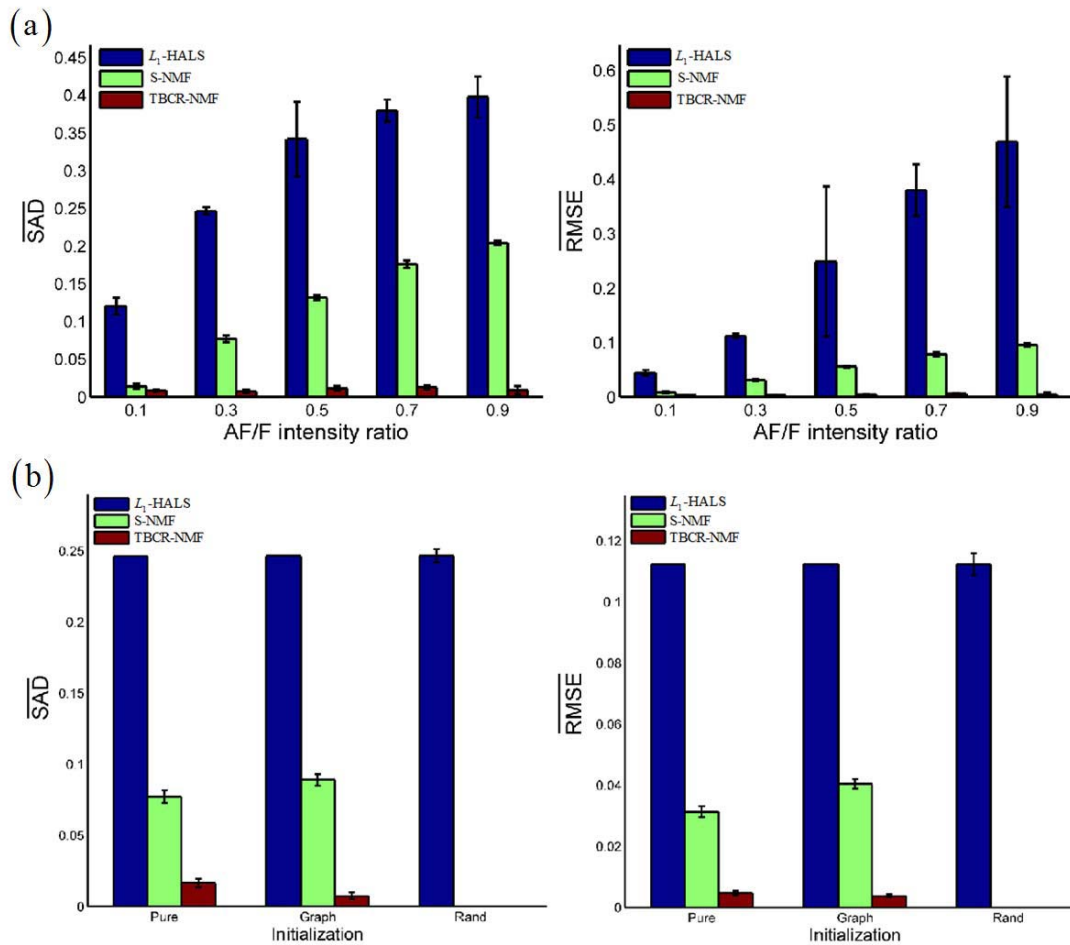


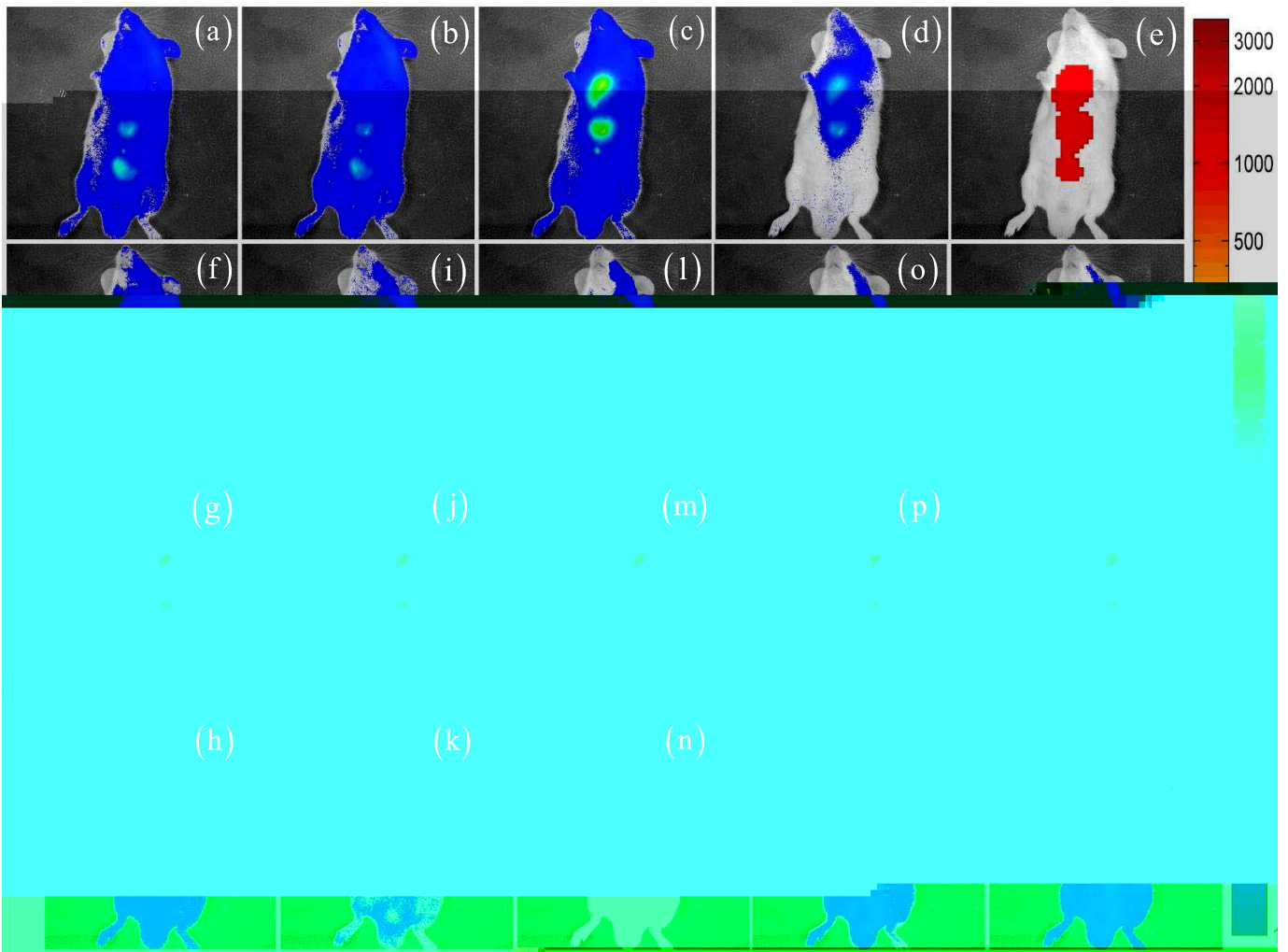
Fig. 4. (a) Algorithm performances for different values of AF/F intensity ratio. (b) Algorithm performances for different initialization methods.

Besides the  $L_1$ -HALS and S-NMF, we also use two All animal experiments in this paper were approved by NMF-based SUM algorithms: nonnegative matrix under our institutional review board. In experiment I, AF488 approximation (NMU)<sup>2</sup> [34] and NMF with  $L_0$  constraint and Alexa Fluor 594 (AF594; Invitrogen, Carlsbad, USA) ( $L_0$ -NMF) [35] for comparison. NMU solves NMF problem fluorescent dyes are diluted to  $0.1 \mu\text{gml}^{-1}$ . AF488 is injected with additional underapproximation constraints  $\|S\| \leq D$  which at the bottom of the body with 20 ng dye, while AF594 is allows to obtain better part-based decompositions, which injected near the neck with the same quantity, and a mixture  $L_0$ -NMF introduces sparseness into all abundances via the each dye with 10 ng is located at the middle portion of  $L_0$ -norm constraint. All algorithms assume that the number of endmembers is 3,  $d_k = 3$ . The TBCR-NMF,  $L_1$ -HALS, with the same depth in tissues. Fig. 5(a) and (d) shows four raw NMU, and  $L_0$ -NMF methods are not initialized with priori fluorescence images acquired at 542, 579, 624, and 716 nm knowledge of calibrated endmember spectra except the spectral bands. The first two images are excited at 474 nm S-NMF method. The parameter for  $L_0$ -NMF, S-NMF, and and the last two images at 565 nm. The calibrated spectra of AF488, AF594, and AF [see Fig. 6(a)] are acquired at these To reduce computation cost, we use Otsu's [36] method for four emission filters by precalibration preprocessing to obtain the mouse body mask with which the same imaging conditions, while the spectrum of AF fluorescence regions of interest, whereby all algorithms are the average spectrum acquired in some chosen regions applied to the fluorescence data within the mask only. For mouse with no fluorescent dyes. Fig. 6(a) displays that the best visual effect, all the observations and unmixed results (spatial distribution of all constituent components) are shown in Fig. 6(b) and (c) also shows the calibrated spectra of AF488, with rainbow pseudocolor and overlaid on the gray-scale AF555, and AF, acquired ex vivo at the 525, 542, 579, photographic image of corresponding mouse. and 624 nm spectral bands for the next *in vivo* fluorescence imaging experiments in the following section.

We first give two *in vivo* BALB/c mouse experiments to validate the proposed method's performance. Fig. 5(e) shows the target/background classification result where the multiple fluorophores are classified as a target group (red color) and separated from the whole background

<sup>2</sup><https://sites.google.com/site/nicolasgillis/code>





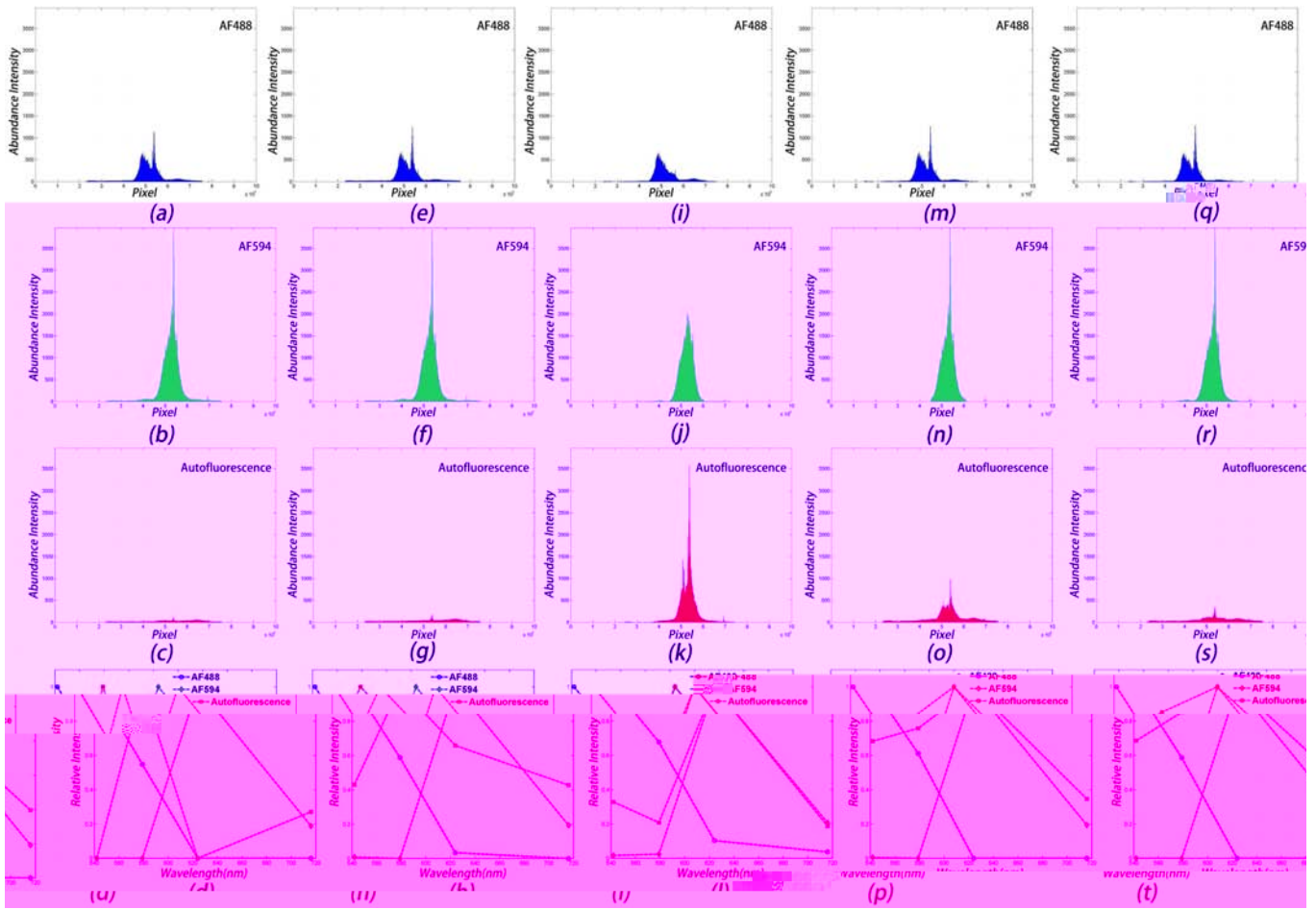


Fig. 7. Abundances (expressed as 1-D vectors) of AF488, AF594, AF, and their spectra from top row to bottom row for experiment I. The unmixed results obtained with (a)D(d) NMU, (e)D(h) L<sub>0</sub>-NMF, (i)D(l) L<sub>1</sub>-HALS, (m)D(p) S-NMF, and (q)D(t) TBCR-NMF.

There are some missing parts of AF488 in the middle portion of the TBCR-NMF [Fig. 7(s)] has slowly varying abundances of BALB/c mouse in Fig. 5(l) for L<sub>1</sub>-HALS, which also of AF. More importantly, the spectra estimated with S-NMF falsely makes the unmixed background AF [Fig. 5(n)] appear sparser and brighter than it actually is. The TBCR-NMF and S-NMF can separate the fluorescence targets from AF in Fig. 5(o)D(q) and Fig. 5(r)D(t), respectively. However, the unmixed results obtained with TBCR-NMF are smoother and clearer than S-NMF.

The unmixed results of abundances (expressed as 1-D vectors) and endmember spectra are illustrated in Fig. 7(a)D(d) for NMU, Fig. 7(e)D(h) for L<sub>0</sub>-NMF, Fig. 7(i)D(l) for L<sub>1</sub>-HALS, Fig. 7(m)D(p) for S-NMF and Fig. 7(q)D(t) for TBCR-NMF, respectively. The TBCR-NMF algorithm obtains more accurate unmixed fluorescence abundances compared with the other algorithms. All algorithms have the highest abundance intensities that correspond to the true pixel positions of fluorescence targets. The abundances of AF488 and AF594 are wide and contain the unwanted AF parts that are not removed with NMU in Fig. 7(a) and (b) and L<sub>0</sub>-NMF in Fig. 7(e) and (f). This AF remainder also can be confirmed by AF's abundances [Fig. 7(c) and (g)] obtained with both algorithms. The L<sub>1</sub>-HALS [Fig. 7(k)] and S-NMF [Fig. 7(o)] have abnormal (too large) values in the abundances of AF, except that

TABLE I

SAD AND  $\overline{\text{SAD}}$  RESULTS ON THE In Vivo EXPERIMENTS I AND II (THE SMALLER VALUES MEAN BETTER RESULTS. THE NUMBER IN BOLD REPRESENTS THE BEST PERFORMANCE)

---

Experiment	SAD	$\overline{\text{SAD}}$
I		
II		

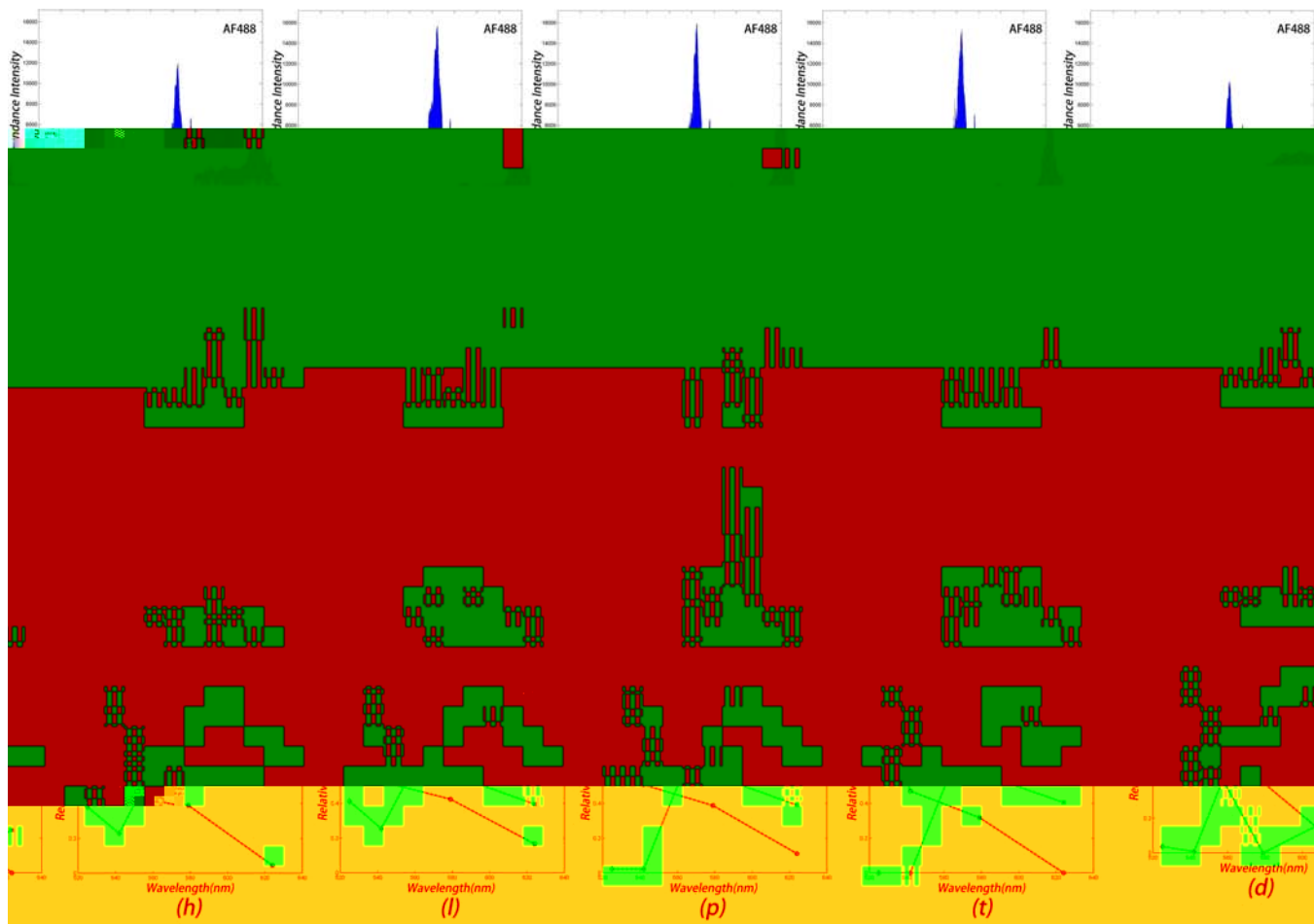


Fig. 9. Abundances (expressed as 1-D vectors) of AF488, AF555, AF, and their spectra from top row to bottom row for experiment II. The unmixed results obtained with (a) NMU, (e)  $L_0$ -NMF, (i)  $L_1$ -HALS, (m) S-NMF, and (q) TBCR-NMF.

The unmixed abundances (expressed as 1-D vectors) and endmember spectra are illustrated in Fig. 9(a)-(d) for NMU, Fig. 9(e)-(h) for  $L_0$ -NMF, Fig. 9(i)-(l) for  $L_1$ -HALS, Fig. 9(m)-(p) for S-NMF and Fig. 9(q)-(t) for TBCR-NMF, respectively. The TBCR-NMF achieves the most accurate unmixed results compared with other algorithms. Particularly, the first row in Fig. 9 displays that AF488 abundance intensities obtained with other algorithms still contain AF parts that are not fully removed. The second row in Fig. 9 shows that the AF parts have made contributions to the AF555 abundances with the NMU,  $L_0$ -NMF and  $L_1$ -HALS algorithms except the TBCR-NMF and S-NMF. The S-NMF has abnormal (too large) values for the AF abundance in Fig. 9(o), while TBCR-NMF can get slowly varying abundances of AF in Fig. 9(s). In general, the unmixed abundances of AF488 and AF555 from the TBCR-NMF algorithm [Fig. 9(q) and (r)] are more sparse than other algorithms. Moreover, the spectra obtained with NMU in Fig. 9(d),  $L_0$ -NMF in Fig. 9(h), and  $L_1$ -HALS in Fig. 9(l) are clearly different from the calibrated spectra in Fig. 6(b). However, the spectra obtained with S-NMF in Fig. 9(p) and TBCR-NMF in Fig. 9(t) are more accurate than other algorithms.

The SAD and the average SAD values of three unmixed endmembers from vivo experiment II are shown in Table I.



Fig. 10. (a)–(d) Raw fluorescence (AF488 and AF647) images for experiment III acquired at the 525, 547, and 624 nm emission filters respectively, the first two images are excited at 474 nm and the last two images at 500 nm. (e) Classification results. The different unmixed results obtained with (f)–(h) BCM-spatial, (i)–(k) SparseTV, (l)–(n) RSFoBa, (o)–(q) S-NMF, and (r)–(t) TBCR-NMF.

includes the total variation regularization to the classical sparse regression formulation to exploit the spatial-contextual information present in the multispectral images. The RSFoBa

TABLE II  
 SAD AND  $\overline{SAD}$  RESULTS ON THE In Vivo EXPERIMENTS III AND IV (THE SMALLER VALUES MEAN BETTER RESULTS. THE NUMBERS IN BOLD REPRESENT THE BEST PERFORMANCE)

Methods	prior knowledge	Experiment III	Ex <sub>4</sub>
---------	-----------------	----------------	-----------------



T. Tian-heng, and T. Li-ming for contributing to the project, and Dr. P. Jin-liang for supporting the experiments in fluorescence imaging. The authors declare that they have no competing interests.

#### REFERENCES

- [1] F. Leblond, S. C. Davis, P. A. Valdžs, and B. W. Pogue, "Pre-clinical whole-body fluorescence imaging: Review of instruments, methods and applications," *J. Photochem. Photobiol. B, Biophys.* vol. 98, pp. 77–94, Jan. 2010.
- [2] F. L. Peña, J. L. Crespo, and R. J. Duro, "Unmixing low-ratio endmembers in hyperspectral images through Gaussian synapse ANMF," *Trans. Instrum. Meas.* vol. 59, no. 7, pp. 1834–1840, Jul. 2010.
- [3] J. Plaza, E. M. T. Hendrix, I. Garc'a, G. Mart'n, and A. Plaza, "On end-member identification in hyperspectral images without pure pixels: A comparison of algorithms," *J. Math. Imag. Vis.* vol. 42, pp. 163–175, Feb. 2012.
- [4] A.-S. Montcuquet, L. Hervž, F. Narro, J.-M. Dinten, and J. I. Mars, "On vivo fluorescence spectra unmixing and autofluorescence removal by sparse nonnegative matrix factorization," *IEEE Trans. Biomed. Eng.* vol. 58, no. 9, pp. 2554–2565, Sep. 2011.
- [5] R. Zdunek, "Regularized nonnegative matrix factorization: Geometrical interpretation and application to spectral unmixing," *J. Appl. Math. Comput. Sci.* vol. 24, no. 2, pp. 233–247, 2014.
- [6] J. Galeano, S. Perez, Y. Montoya, D. Botina, and J. Garz'n, "Blind source separation of ex-vivo aorta tissue multispectral images," *Biomed. Opt. Exp.* vol. 6, no. 5, pp. 1589–1598, 2015.
- [7] J. Xu et al., "Sparse non-negative matrix



Chen Hu received the B.S. degree in biomedical Engineering from Xi'an Jiaotong University, Xi'an, China, in 2011, and the M.S. degree from Shanghai Jiao Tong University, Shanghai, China, in 2014.

Shaosen Huang received the B.S. degree and the M.S. degree in biomedical engineering from Shanghai Jiao Tong University, Shanghai, China, in 2011 and 2013, respectively.